2006-01-0896

Examination of Pitting Fatigue in Carburized Steels with Controlled Retained Austenite Fractions

Ryan M. Wagar, John G. Speer, David K. Matlock, and Patricio F. Mendez
Colorado School of Mines

ABSTRACT

The effects of several variables on pitting fatigue life of carburized steels were analyzed using a geared roller test machine (GRTM). The material variables that were primarily used to influence retained austenite include aim surface carbon concentration (0.8 % and 0.95 %), alloy (SAE 4320 and a modified SAE 4122), and cold treatment (performed on one material condition per alloy). Testing variables included contact stress in addition to a variation in lambda ratio (oil film thickness/surface roughness), arising from variation in roughness among the machined surfaces. Test results are presented, and differences in performance are considered in terms of material and testing variables. A primary observation from these results is an improvement in contact fatigue resistance apparently arising from cold-treatment and the associated reduction of retained austenite at the surface.

INTRODUCTION

Fatigue behavior of carburized gear steels has been examined extensively in the past (1). Specifically, bending fatigue of these steels has been a primary area of research, and carburizing treatments have been developed to increase the bending fatigue resistance of gear steels. Contact fatigue is an important failure mechanism in some gears, and a better understanding of the contact fatigue behavior of carburized gear steels needs to be developed.

Many researchers have studied contact fatigue, although most of the publicly available research has been in the area of rolling contact fatigue. One reason that much more research has been performed on rolling contact fatigue is the relative simplicity of laboratory testing as compared to the study of the fatigue under contact conditions that occur in gear operation, i.e. combined rolling and sliding. In contrast, pitting fatigue is often evaluated on actual gears, rather than simulative specimens.

Fatigue failure from the contact conditions present in gear operation manifests itself as a pit. Pitting fatigue involves spalling that increases vibration and wear, which decreases the load a tooth can take, until fracture occurs (2). Although some observations have been made about the causes of pitting in gears, further understanding would be helpful (3).

Many factors affect the resistance a gear has to pitting fatigue. Intergranular oxides (IGO's) that form along prior austenite grain boundaries during carburizing and inclusions in the steel are often nucleation sites for fatigue cracks (4). Finer prior austenite grain sizes, which are well known to increase bending fatigue resistance, may help with pitting fatigue by limiting segregation of phosphorus, precipitation of cementite, and the interaction between the two, all of which increase the likelihood for cracks to initiate at grain boundaries (5). Low elastohydrodynamic (EHD) lubrication has been shown to lead to scuffing (6) and shortened pitting fatigue lives (7). Other factors like contact stress, geometric tolerances, and carburizing type can also affect pitting fatigue.

The purpose of this study is to evaluate the effect of retained austenite fraction on pitting fatigue life. A common belief is that retained austenite increases fatigue resistance at low cycles but reduces fatigue strength under conditions where higher numbers of cycles are experienced (8). This belief results from *bending* fatigue studies that relate levels of retained austenite to endurance limit. Nakamura *et. al.* report that pitting fatigue resistance improves with increasing hardness for higher cycles (3). Since higher austenite contents lead to lower hardness values (8), it may be reasonable to expect retained austenite to have a detrimental effect in the high cycle regime. However, Shaw, Abudaia, and Evans argue that "gear materials

made from steels with a high level of retained austenite and a low case hardness showed high fatigue resistance and good performance" (9). In addition, they argue that the material has good high-cycle pitting resistance. With respect to low-cycle fatigue, high levels of retained austenite are beneficial at the higher stresses involved, because the high ductility of the austenite reduces the negative effects of debris in the oil and asperities between gear teeth (2). Furthermore, the austenite is converted to martensite through stress and strain induced transformation causing a volume expansion linked to compressive residual stresses. The effect of retained austenite on sliding and rolling contact fatigue in carburized steels has not been fully established and is, therefore, a key test variable for this research.

In order to control retained austenite, several methods were employed in this investigation. Surface carbon was controlled by using two different gas carburizing cycles, where the cycle targeting a higher surface carbon should yield greater amounts of retained austenite. (A vacuum carburizing cycle was run as well, and the results will be reported at a later date.) Retained austenite was controlled further by using two different steels with different alloy levels and thus carbon equivalencies. Another technique used was a sub-zero treatment which increases the driving force to transform austenite to martensite.

Sub-zero treatments are useful in applications where deformation-induced martensite transformation could jeopardize the geometry of a part (5). This applies to any part that needs to be of exact dimensions and unchanged by the transformation of retained austenite. Previous studies show diminished bending fatigue performance among steels that were cryogenically treated with a temper before and after the cryogenic treatment (5). These sub-zero treatments have been reported to lead to development of *tensile* residual stresses in the remaining austenite regions, promoting crack initiation (10). The cracking problem with sub-zero treatments can reportedly be alleviated by grain refinement and the use of nickel (nickel can increase fracture toughness to offset the decrease from subzero treatment) (2, 5). In the present study, a single temper after cold-treatment was included.

MATERIALS AND EXPERIMENTAL PROCEDURE

MATERIALS

Two commonly used carburizing steel grades were selected for this study (SAE 4320 and 4122 M). Table 1 summarizes the chemical compositions of the selected steels. The 4122 M grade was selected because of its widely accepted use as a gear steel. The 4320 grade was selected, not only because of its wide use as a gear steel, but also because the higher nickel content in the 4320 steel grade can influence fracture behavior and retained austenite levels. The other alloying differences are incidental, and their effects will be discussed later.

Table 1: Chemical Compositions of the Steels Selected for Pitting Fatigue Testing (wt. %).

Steel	C	Mn	P	S	Si	Cr	Ni	Mo	Cu	Al
4320	0.18	0.62	0.014	0.031	0.21	0.51	1.83	0.25	0.15	0.034
4122M	0.21	0.90	0.011	0.026	0.15	0.73	0.27	0.27	0.26	0.024

GEARED ROLLER TEST MACHINE

For the purpose of comparing the steels with respect to rolling/sliding contact fatigue, a geared roller test machine (GRTM) was utilized. All of the GRTM testing was performed at Caterpillar Technical Center.

Figure 1 shows a simple schematic of a GRTM. The GRTM is a machine that applies a load to two surfaces that are rolling and sliding against each other in a controlled fashion. The two surfaces include the test roller and the load roller, which were paired based on similarity of surface roughness. A test roller was the test specimen prepared from the experimental alloys and carburized to specifications. A test roller is approximately 25.4 mm (1.0 in.) in diameter and 127 mm (5.0 in.) in length. The test roller was press fit into the lower shaft so that only the test portion remains exposed (about 25 mm in the middle of the test roller surface was left as heat treated—the remainder was ground to facilitate the press fitting process). A load roller was approximately 127 mm (5.0 in.) in diameter. Each load roller was carburized and then machined to provide a crowned surface (so as to eliminate edge effects) and limit variability from load roller to load roller. The load roller was press fit onto the upper shaft.

Once the shafts were assembled, the test could be started. Using bearings to support the revolution of each of the shafts, the lower shaft was driven from one end while a gear set at the opposing end of the shaft drove the upper shaft. The test roller and load roller were in contact with each other through an oil supply that was maintained with oil jets. The oil was heated and the temperature of the oil was measured by a thermocouple near the contact of the two rollers. The oil temperature was further controlled by water cooling that was automatically adjusted based on the thermocouple readout. The load on the upper shaft was applied pneumatically, in accordance with the desired contact stress. An accelerometer linked to the upper shaft detected vibration. When a specified vibration was reached (indicating sample failure), the machine was automatically shut off. If the sample did not exhibit failure after a specified vibration was reached, the machine was once again restarted. Once the sample exhibited a failure (in the form of surface cracks or a pit of any size), the test was terminated.

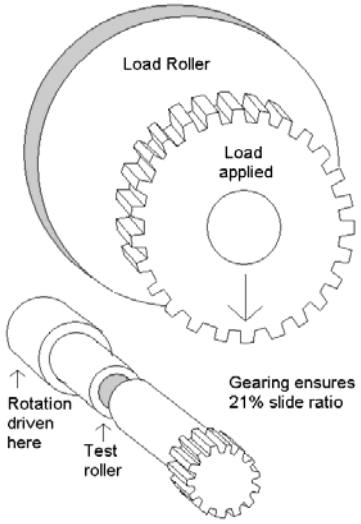

Fig. 1: Schematic illustration of GRTM test configuration.

The test matrix utilized for this project involved nine replicate tests per group run at 1200 RPM, 110 °C (230 °F), and 3.2 GPa contact stress. The lambda ratio (oil film thickness/root mean square roughness of the load and test roller) for each test was influenced by the surface roughness of the load and test rollers, as well as the oil temperature, RPM, contact stress, and slide ratio. When possible, these variables were held constant, although some variations were naturally encountered, such as in the load/test roller surface topography. Although the load and test rollers were paired by similarity of roughness, no effort was made to adjust the oil film thickness to accommodate roughness variations between paired sets. Consequently some variability in initial lambda ratio (i.e. lambda ratio at the beginning of a test) was involved in this testing, though even greater variations were encountered due to changes in the roller surfaces during testing, and these changes are typically not considered in contact fatigue testing.

DATA NORMALIZATION

When a test was completed, the data were normalized to remove the influence of variation in lambda ratio among the test replicates (11). The life data were then plotted against lambda ratio, and a straight line that fits the data using the least squares method was drawn (Fig. 2). Based on the slope of the regression line, the regressed life value at lambda = 0.4 was used to represent "equivalent life." This normalization process allowed the equivalent contact fatigue life values to be compared, yielding comparisons between test groups.

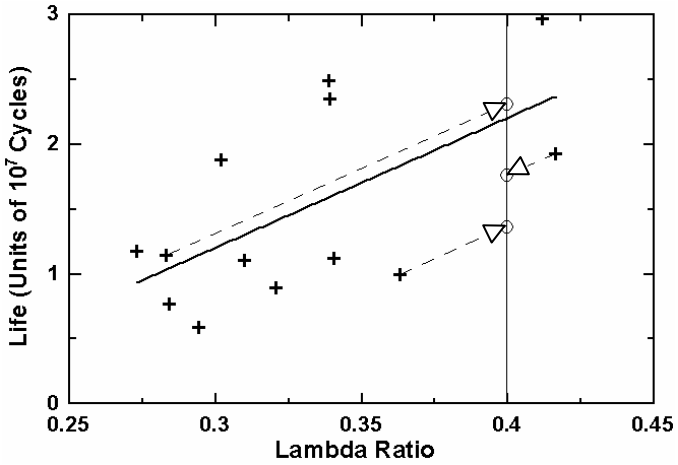

Fig. 2: The normalization process can provide equivalent life values for a given set of data at any lambda ratio. Life data are plotted against their lambda ratio. The least squares method was used to generate a line of best fit (solid line). The data were then "adjusted" as shown to yield an equivalent life (dashed lines with arrows).

WEAR INVESTIGATION

Since retained austenite is central to this study and may affect the wear properties of a carburized steel under contact conditions, the amount of wear was tracked on each sample. A two dimensional surface profile was measured before testing on each sample. After testing, the surface profile of each sample was measured again. The unworn part of the post-test scan was matched with the ends of the pre-test scan, and a wear track depth for the sample was then determined.

CARBURIZING

CARBURIZING AND POST-CARBURIZING CYCLES

Gas carburizing was performed on the test rollers with an aim surface carbon of 0.95% (high surface C) or 0.80% (low surface C) using a commercial production furnace. All carburizing cycles were performed at 927 °C (1700 °F) followed by a 30 minute equalize period at 840 °C (1544 °F). The quench was performed in oil held at 47°C (117 °F) with full agitation for 15 minutes. One of the 0.95 % C aim surface carbon conditions also included a four hour cold treatment at –80 °C (-112 °F) after quenching. All the test rollers were then tempered at 150 °C (302 °F) for 2 hours. The target case depth was 1-1.2 mm.

CARBURIZING RESULTS

Several methods were used to characterize the results of the carburizing process. Step bars (carburized bars that have layers removed for carbon profile analysis of a cycle) were included to determine the case carbon profile. The step bar analysis provided near surface carbon content at a given measured depth (Table 2). Due to a smaller step bar diameter, the high surface C

4320 step bar needed to have a thicker layer removed for carbon analysis, causing a greater depth of measure (this can be seen in the greater depth of measure of the high C 4320 material conditions). Figure 3 shows the carbon profiles for the 4320 alloy confirming increased surface carbon of the high surface C carburizing procedure with respect to the low surface C carburizing procedure.

Table 2: Aim Surface Carbon Content (SCC) and Actual Near Surface Carbon Content of Heat Treated Specimens.

Steel Grade	Aim SCC	Cold-Treat	Carbon Content wt. %	Depth of Measure (mm)
4320	0.95%	Yes	0.84%	0.0457
4320	0.95%	No	0.84%	0.0457
4320	0.80%	No	0.73%	0.0146
4122 M	0.95%	Yes	0.91%	0.0108
4122 M	0.95%	No	0.91%	0.0108
4122 M	0.80%	No	--	--

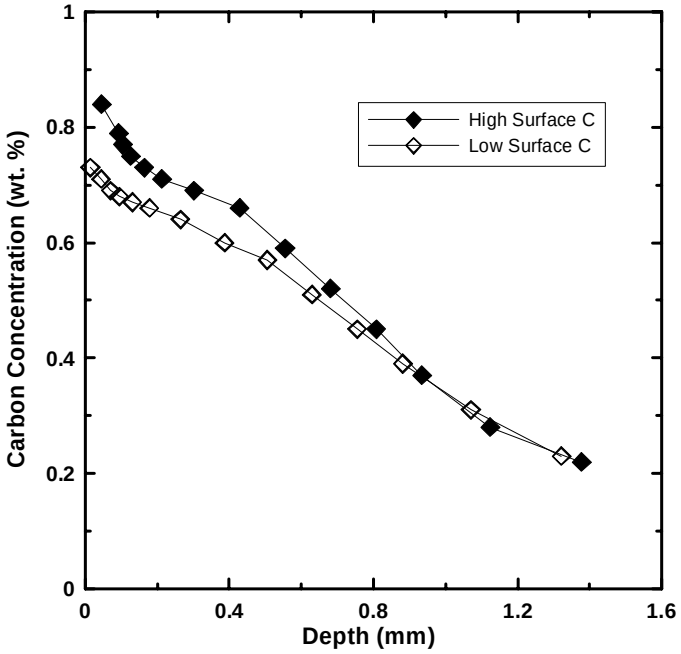

Fig. 3: Carbon profiles of the 4320 grade determined from step bar after carburizing.

Cylindrical test pieces of each material were included in the full heat-treatment cycle to determine the hardness profiles and microstructures created by the cycles. Table 3 shows the hardness profiles for each material condition. The cold-treatment generated a higher surface hardness and the 4320 grade exhibited a reduced hardness at depths of 0.8 mm and greater (Figure 4).

Table 3: Hardness (Rockwell C) at Varying Depths of Test Pieces for Each Heat Treatment.

Depth (mm)	4122 M			4320		
	0.80%	0.95%		0.80%	0.95%	
	As Carb	As Carb	Cold Treat	As Carb	As Carb	Cold Treat
0.2	64.8	64	66.2	62.7	63.3	65.8
0.3	64.4	64.6	65.9	62.8	63	66.3
0.4	64.7	64.2	64.8	62.7	62.9	65
0.5	63.6	64.6	64.3	62.3	62.8	64.6
0.6	62.5	64.4	64.2	60.7	62.9	64.1
0.7	62.4	63.8	62.6	58.8	62.1	62.8
0.8	59.9	62.5	61.3	58.1	60	60.4
0.9	58.1	60.5	58.5	55	57.3	56.6
1	56.3	57.1	55.1	54.2	54.8	54.3
1.1	53	54.4	53.6	51.2	52.2	51.3
1.2	51.9	51.4	50.8	49.9	50.2	50.1
1.3	49.1	50.8	50.1	49	49	48.8

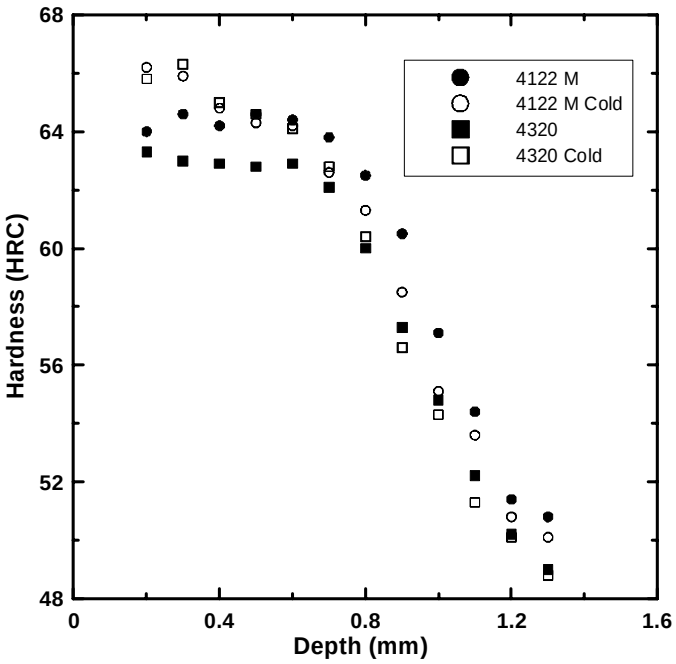

Fig. 4: Hardness profiles of the high surface carbon specimens comparing the hardness of samples that were cold-treated with those that were not cold-treated.

Retained austenite profiles were determined using a chemical thinning process in combination with x-ray diffraction (XRD) on the end portion of a test roller from each heat treatment. Table 4 shows the results of the retained austenite profiling. Figure 5 compares the retained austenite profiles for the two alloys. In both alloys, the retained austenite fraction increased slightly

from the surface inward to a given depth where it reached a maximum before the fraction decreased with increasing depth. This subsurface maximum in retained austenite has been reported previously (12, 13). Notably, in the steel grades that were studied in this research, the carburizing treatments and cold-treatment produced substantial variation in the retained austenite levels. The cold-treated samples exhibited a substantial reduction of retained austenite when compared to the as-carburized condition. Also, the low surface carbon content specimens showed lower retained austenite when compared with the high surface carbon specimens that were not cold-treated. A comparison between the two alloys (Figure 4a vs. 4b) does not show an increased amount of retained austenite in the 4320, which would have been expected because of its higher Ni content. Lastly, the microstructures of a sample from each heat treatment showed very similar intergranular oxidation depth (average at approximately 18 μm for each sample) and the very minimal presence of carbides.

Table 4: Retained Austenite Fractions.

	4122 M			4320		
	Low C	High C		Low C	High C	
Depth (mm)	As Carb	As Carb	Cold Treat	As Carb	As Carb	Cold Treat
0	0.12	0.14	0.07	0.13	0.17	0.05
.074-.093	0.27	0.36	0.06	0.19	0.28	0.09
.144-.177	0.23	0.29	0.06	0.22	0.28	0.08
.226-.247	0.12	0.20	0.03	0.16	0.21	0.06
.303-.313	0.11	0.14	0.05	0.09	0.18	0.04

RESULTS

CONTACT FATIGUE TESTING

After normalizing all of the data from tests run at 3.2 GPa to a lambda ratio of 0.4, the average of the equivalent life values for each test group was obtained and the results are summarized in Figure 5. There are many factors that influence the fatigue life of these samples, such as the use of different test machines and sample holders, variation in proximity of the thermocouple to the contact surface (which could cause oil heating past the point of breakdown), and differences in continuity of testing (many tests shut off several times before failure and had to be restarted). Hence, small differences in equivalent fatigue life are likely not significant. From the results in Figure 6, it is clear that cold-treatment is beneficial to the contact fatigue life of both alloys for the high surface carbon condition. (Cold-treatment was not evaluated for low surface carbon conditions.) The low surface C condition proved to be a good heat treatment for the 4122 M alloy as it significantly outperformed the high surface C condition. However, for the 4320 alloy the low surface C heat treatment did not outperform the high surface C. Comparing alloys, the 4320 cold-treated sample slightly outperformed the 4122 M cold-treated sample, while the low surface C heat treat for the 4122 M alloy clearly outperformed the low surface C for the 4320.

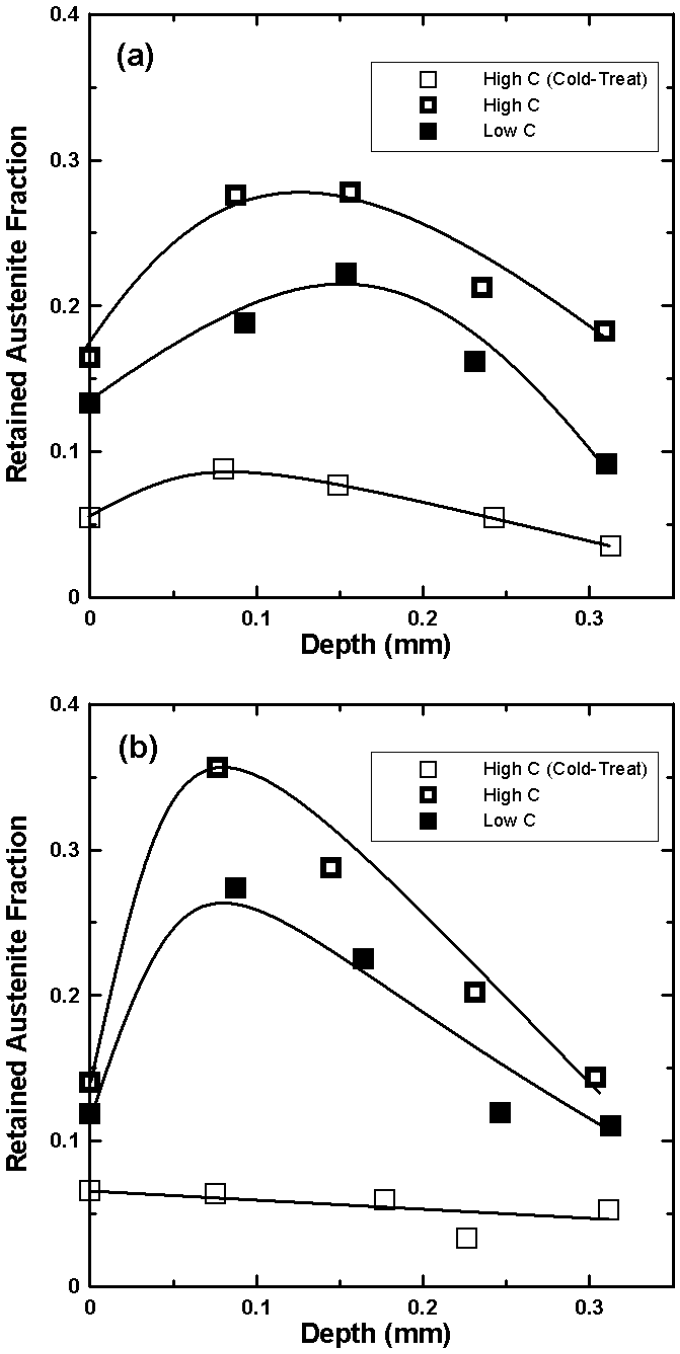

Fig. 5: Retained austenite vs. depth determined by XRD. (a) for the 4320 steel grade and (b) for the 4122 M steel grade.

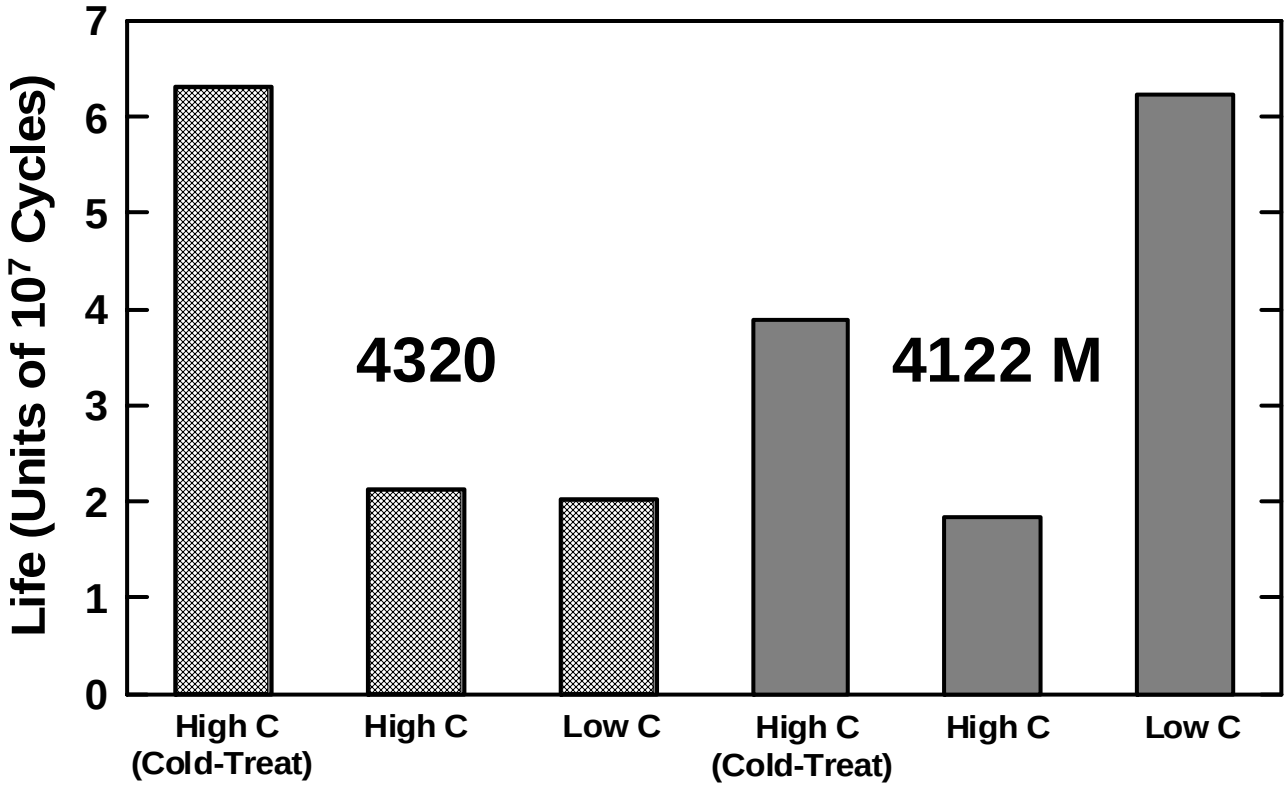

Fig. 6: Comparison of average equivalent life from fatigue testing at a contact stress of 3.2 GPa.

DISCUSSION

The gas carburizing process yielded microstructures, hardness profiles, and carbon profiles as expected. The retained austenite measurements also yielded profiles as expected, except that a higher retained austenite fraction was not found to result from the higher Ni content of the 4320 alloy. When analyzing the two alloys with respect to the martensite transformation behavior, an identical carbon profile for both alloys would lead to an M_s temperature for the 4320 alloy about 16 °C lower than that of the 4122 M alloy. This value is obtained using the Andrews linear expression for M_s: M_s (°C) = 539 - 423 C – 30.4 Mn – 12.1 Cr – 17.7 Ni – 7.5 Mo (14). Table 5 shows a comparison of calculated and measured retained austenite fractions. The M_s temperature for each material condition was calculated using the Andrews linear expression. Although the M_s temperature was expected to be 16 °C lower for the 4320 relative to the 4122 M, the M_s temperatures were actually much more similar because the carbon content was slightly higher in the 4122 M than the 4320 at the depth where measurements wer made. T_{cold} represents the coldest temperature to which each material condition was exposed, and the undercooling (ΔT) is the difference between the M_s temperature and T_{cold}. The calculated RA value was determined from the Koistinen and Marburger expression for the athermal transformation kinetics of martensite formation: $f = 1 – \exp(-0.011\Delta T)$ where f is the fraction of martensite (14). The similarity between calculated and measured retained austenite fractions in Table 5 indicates that higher nickel content in the 4320 is essentially compensated by the higher carbon content of the 4122 M.

Table 5: Calculated and Actual Retained Austenite RA) Fractions with Martensite Start Temperatures and Undercooling (ΔT)

	4320			4122 M	
	Low C	High C		High C	
	As Carb	As Carb	Cold Treat	As Carb	Cold Treat
M_s	192 °C	146 °C	146 °C	149 °C	149 °C
T_{cold}	20 °C	20 °C	-80 °C	20 °C	-80 °C
ΔT	172 °C	126 °C	226 °C	129 °C	229 °C
Calc. RA	0.15	0.25	0.08	0.24	0.08
Actual RA	0.19	0.28	0.09	0.36	0.06

The normalized contact fatigue life data indicated that the materials exhibit increased length of life with reductions in retained austenite. The lone exception to this statement comes when comparing the non cold-treated samples from the 4320 alloy and the reason for this difference in performance relative to retained austenite is unclear, pending further analysis of the test specimens (SEM analysis of the failed surfaces is underway). However, it is very clear that the cold-treatment caused a change in the material that enhanced pitting fatigue resistance. The enhancement is especially strong for the 4320 alloy where a higher

amount of Ni is present. Since Ni increases the resistance of steel to crack propagation, additional Ni may have helped to reduce pitting susceptibility due to cold-treatment (5).

When analyzing contact fatigue life vs. wear track depth, a clear correlation can be shown. Figure 7 shows a wear track from a test roller. The depth of this wear track is significantly less than the depth of any of the formed pits, and the wear track in Figure 7 matches the original crown profile of a load roller. Because the load roller was able to wear away the test roller surface to match its crown, it is clear that this particular test roller showed low wear resistance. Low wear resistance was found to be correlated with a shorter life. Figure 8 plots fatigue life in millions of cycles against maximum wear track depth on a log-log plot for all of the tests run at 3.2 GPa. The inverse relationship suggests that the decreased resistance to wear may be a mechanism that causes earlier failures (i.e. pits) in some test samples. Further the wear may have penetrated the surface of the test roller, thereby exposing surfaces with reduced pitting fatigue resistance, which in turn fail more quickly. Alternatively, one might hypothesize that the samples that experienced early (undetected) pitting also exhibited high wear, as a consequence of early pitting.

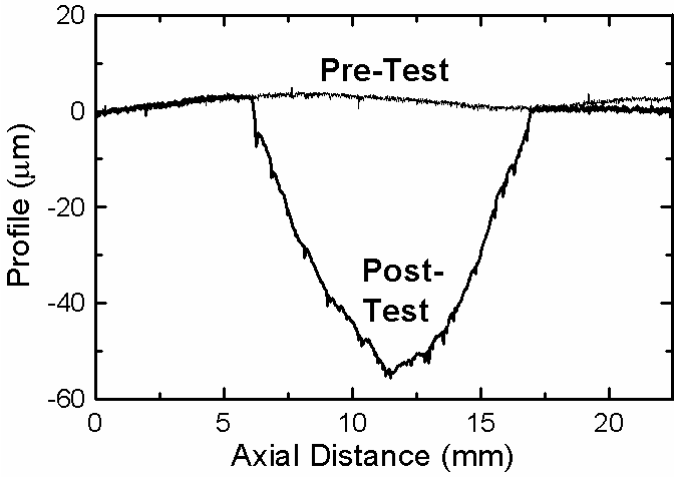

Fig. 7: Wear track of tested roller superimposed on pre-test surface scan of same test roller. The profile of this wear track closely matches the crown of a load roller.

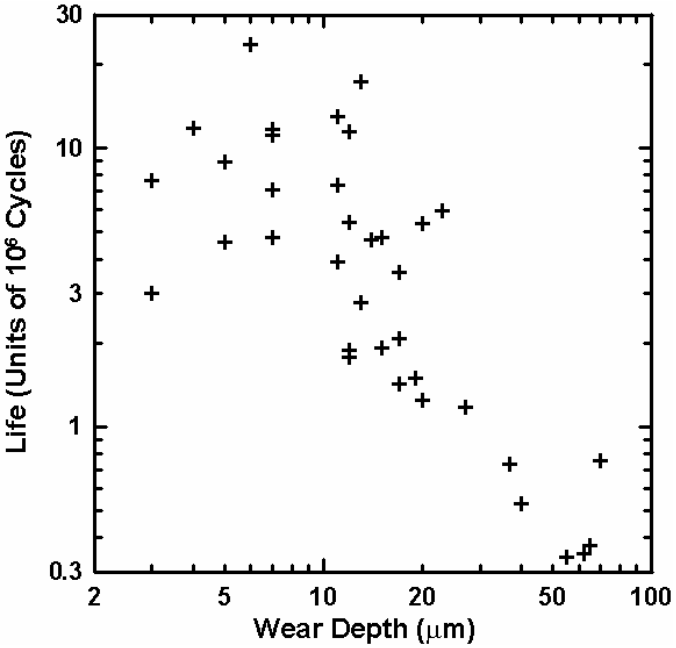

Fig. 8: Contact fatigue life vs. maximum wear track depth suggesting that wear may have a detrimental effect on pitting fatigue life. This figure includes data from all tests run at 3.2 GPa.

SUMMARY

The following conclusions and inferences can be drawn from the results of this study:

1. Cold-treatment and the associated reduction of retained austenite and increased hardness near the surface promote contact fatigue resistance in gas carburized steels with surface carbon values near 0.9%.

2. Carburized surfaces designed for contact fatigue that have decreased wear resistance tend to exhibit decreased pitting resistance.

ACKNOWLEDGMENTS

The authors acknowledge the support of the Advanced Steel Processing and Products Research Center, a NSF-Industry-University cooperative research center at the Colorado School of Mines. The assistance of Caterpillar Inc., and in particular Mike Shockley, Steven Cross, and Scott Johnston is gratefully acknowledged for lending significant support and guidance throughout the project.

REFERENCES

1. J.P. Wise, D.K. Matlock, G. Krauss, “Bending Fatigue of Carburized Steels”, *Heat Treating Progress*, August/September 2001, pp. 33-41.

2. G.P. Cavallaro, T.P. Wilks, C. Subramanian, K.N. Strafford, P. French, J.E. Allison, “Bending Fatigue and Contact Fatigue Characteristics of Carburized Gears”, *Surface and Coatings Technology* 71, 1995, pp. 182-192.

3. T. Nakamura, T. Hanyuda, M. Yoshida, Y. Murakami, “Development of Pitting Resistant Steel for Transmission Gears”, SAE Paper No. 010827, 2001.

4. T. Kimura, A. Hatano, N. Uchiyama, M. Yoshida, S. Asano, “Improvement in Pitting Resisatnce of Transmission Gears by Plasma Carburizing Process”, SAE Paper No. 940727, 1994.

5. G. Krauss, “Bending Fatigue of Carburized Steels”, *ASM Handbook,* Vol. 19, 1996.

6. O.O. Ajayi, J.G. Hersberger, J. Zhang, H. Yoon, G.R. Fenske, “Microstructural Evolution During Scuffing of Hardened 4340 Steel—Implication for Scuffing Mechanism”, *Tribology International* 38, 2005, pp. 277-282.

7. H. Lin, R.R. Binoniemi, G.A. Fett, M. Deis, “Contact Fatigue Tests and Contact Fatigue Life Analysis”, SAE Paper No. 010795, 2001.

8. M.A. Zaccone, J.B. Kelley, G. Krauss, “Strain Hardening and Fatigue of Simulated Case Microstructures of Carburized Steels”, *Industrial Heating*, September 1989, pp 38-51.

9. B.A. Shaw, F.B. Abudaia, J.T. Evans, “Characterization of Retained Austenite in Case Carburized Gears and Its Influence on Fatigue Performance”, *Heat Treating: Proceedings of the 20th Conference*, Vol. 1, ASM International, 2000, pp.18-23.

10. G.P. Cavallaro, C. Subramanian, “Fatigue Aspects of Case Hardened Gears”, *Gear Technology*, March/April 1999, pp. 18-23.

11. S.M. Cross, Private Communication, Caterpillar, Inc., 2004.

12. P. Rangaswamy, C.P. Scherer, M.A.M. Bourke, “Experimental Measurements and Numerical Simulation of Stress and Microstructure in Carburized 5120 Steel Disks”, *Materials Science and Engineering A,* Vol. 298, 2001, 158-165.

13. J.J. Spice, “Optimized Carburized Steel Fatigue Performance as Assessed with Gear and Modified Brugger Fatigue Tests”, M.S. Thesis, Colorado School of Mines, 2002, p. 48.

14. G. Krauss, *Steels: Heat Treatment and Processing Principles*, ASM International, 1990, pp. 53-55.